

Imaging of $z \sim 2$ QSO host galaxies with the Hubble Space Telescope ¹

J.B. Hutchings, D. Frenette

Herzberg Institute of Astrophysics, National Research Council of Canada,
Victoria, B.C. V8X 4M6, Canada
john.hutchings@nrc.ca

R.Hanisch, J.Mo²

Space Telescope Science Institute,
3700 San Martin Drive, Baltimore, MD21218
hanisch@stsci.edu,jinger@stsci.edu

P.J. Dumont, D.C. Redding

Jet Propulsion Laboratory,
4800 Oak Grove Drive, M/S 306-438, Pasadena, CA91109
david.c.redding@jpl.nasa.gov,philip.j.dumont@jpl.nasa.gov

S.G.Neff

Code 681, NASA Goddard Space Flight Center, Greenbelt, MD20771
neff@stars.gsfc.nasa.gov

ABSTRACT

We report on deep imaging in 2 filters with the PC2 camera of HST, of five QSOs at redshift ~ 2 , with a range of optical and radio luminosity. The observations included a suite of PSF observations which were used to construct new PSF models, described elsewhere by Dumont et al (2001). The new PSF models were used to remove the QSO nucleus from the images. We find that the host galaxies have resolved flux of order 10% of the QSO nuclei, and are generally luminous and blue, indicating active star-formation. While most have clearly irregular morphologies, the bulk of the flux can be modelled approximately by an $r^{1/4}$ law. However, all host galaxies also have an additional

¹Based on observations with the NASA/ESA Hubble Space telescope, obtained at the Space Telescope Science Institute, which is operated by the Association of Universities for Research in Astronomy (AURA) Inc, under NASA contract NAS5-26555.

²Computer Sciences Corporation

approximately exponential luminosity profile beyond a radius about 0.8 arcsec, as also seen in ground-based data with larger telescopes. The QSOs all have a number of nearby faint blue companions which may be young galaxies at the QSO redshift. We discuss implications for evolution of the host galaxies, their spheroidal populations, and central black holes.

Subject headings: quasars – galaxies:high-redshift

1. Introduction

There have been several investigations of QSO host galaxies at redshift 2 and higher, using 4m class telescopes (with and without adaptive optics image correction), and with the Hubble Space Telescope. Many of these are reviewed by Hutchings (2001a). Heckman et al (1992) and Lehnert et al (1992) were the first to discover that high redshift QSO hosts were both large and luminous (particularly of radio-loud QSOs), and unlike galaxies in the present-day universe. However, there is a range of host galaxy sizes and luminosities, and it is not easy to study their detailed morphology and colour because of size, redshift dimming, and the presence of the bright central QSO nuclei. In general, however, the QSO hosts become more luminous and compact with increasing redshift, and are found in regions of enhanced faint galaxy counts. There have been claims regarding the host morphology, based on fits to luminosity profiles of the hosts after removal of the central source (e.g. Kukula et al 2001, McLure et al 1999).

The host galaxies of higher redshift QSOs are of interest for several reasons. QSOs show strong cosmic evolution in their population, luminosity, and radio morphology, and we wish to see how the triggering and fuelling of the QSO episodes causes this evolution. Seen over large redshift ranges, the QSO hosts must undergo significant evolution as galaxies, and offer an opportunity to study evolution of galaxy star-formation, stellar populations, merging, and morphology changes in addition to the nuclear activity. It is clear from local galaxy studies that the central black hole mass is closely related to the spheroidal stellar population, so that we may seek to understand how this population forms and evolves, as well as how the central black hole forms and grows with time. We may also measure the central mass independently by the width of the broad emission lines in the QSO nucleus, providing another link to galaxy and black hole evolution.

The results reported here are from a program proposed in 1995, when these studies were new, with a small total sample. As table 1 shows, the observations were not performed until several years later, and other studies had been undertaken. The sample chosen was intended

to cover a range of luminosities in both optical and radio, with some complementary ground-based coverage, and restricted to a small redshift range close to 2. We describe below further details of the observational procedure. We are particularly concerned with accurate modelling and removal of the central point spread function (PSF), on which many of the above conclusions rest.

2. Observations

The observations were carried out as a delayed cycle 6 HST program, and are listed in Table 1. The QSOs were centred in the PC CCD of the WFPC2, and exposed for about 5000 sec in each of the F606W and F702W filters, using several readouts at each filter, to enable cosmic ray removal and to avoid saturation in the nuclear pixels. The rest wavelengths sampled with the filters are in the range 1800 to 2300Å, so are sensitive to young stellar populations. In this paper we refer to the filters and magnitudes as R and I, since the conversions are within the measuring errors of our results.

The images from each QSO were combined and cosmic rays removed in the usual way. No unusual problems were encountered and there were few saturated pixels to deal with. These occurred in the image centres where we have no resolved information. The pixels were replaced with values from scaled PSF images, and were given zero weight in the PSF removal process described below. Obvious bad pixels and cosmic ray pixels were interpolated across in the QSO images.

In addition to the QSOs, a set of PSF observations was made of the star Feige 23, chosen to have an SED in the optical similar to the redshifted QSOs in the program. The PSF observations involved a range of exposure times and dither positions around the centre of the PC field, and were used to generate a model for the PSF for the QSOs.

The PSF observations consisted of four sequences of exposures of a star in each of the two filters. These four sequences were at four field positions: the center and the vertices of a triangle surrounding the nominal PC chip position for the QSOs. The triangle was ~ 3 arcsec on a side, to match the nominal positioning accuracy of targets on the WFPC2 focal plane, oriented at an angle with respect to the CCD rows and columns, to provide both minimum overlap of PSF diffraction features and maximum prescription retrieval fitting leverage in determining alignment parameters. Each exposure sequence contained pairs of exposures with durations of 0.23 sec, 4 sec, and 100 sec. The sequences were chosen to avoid pixels affected by the residual image from previous saturated exposures.

The paired exposures were used to both minimize the effect of noise in the prescription

retrievals and to identify cosmic ray events. The shorter exposures were designed to properly expose the PSF core and enable accurate registration of the PSF with the QSO cores. The 0.23 seconds is the minimum WFPC2 exposure for which the PSF characteristics are unaffected by the shutter flight time. This range of exposure times provided measurements of PSF features over the dynamic range of interest in the the science observations; PSF features that are factors of 10^4 and 10^5 weaker than the core were measured at S/N approximately 35 and 8.5 respectively.

3. Point spread function removal

The PSF modelling work required for this project was carried out as described in detail by Dumont et al. (2001). We also constructed empirical PSFs from the Feige 23 observations, and Tiny Tim PSF models for the QSO locations in the PC (Krist 1995). However, our analysis was done entirely with the Dumont et al. model PSFs, as these resulted in significantly cleaner removal of PSF structures.

The Dumont et al PSFs use a hybrid approach to modelling the HST optical system and WFPC2 PC camera, by combining prescription retrieval to solve for the primary optical components, and phase retrieval to compute a "mirror map" giving deviations in the HST primary mirror from the nominal prescription. The initial prescription (low-order Zernike coefficients) and mirror map were estimated using a series of out of focus images (generated by relocating the secondary mirror) obtained from the HST archive. The prescription was refined by refitting parameters known to vary (secondary mirror position) and known to be dependent on the particular observation (object position in field of view, object intensity, background) and taking into account the object's spectral type and filter bandpass.

The actual PSF models used were ultimately chosen by matching the inner structure and main diffraction spikes in the PSF models with those in the QSO images, as described below. The models were computed with a pixel size eight times smaller than the actual observations, allowing us to make sub-pixel offsets without introducing sampling errors. The final parameters that were adjusted in the PSF models were a) the SED and emission line flux of the program QSOs within each filter bandpass, based on published spectra or the broad-band colours and a 'standard' QSO spectrum, and b) the optical offset of the secondary mirror.

It was found that the flux distribution within the filter bandpass is not a critical PSF issue, with very small changes between a flat SED and one that reflects the continuum and emission lines within the bandpasses. The principal differences between the filter bandpasses

are the scale changes in the PSF structure that are caused by the mean wavelength of the bandpass.

On the other hand, the optical offset of the HST secondary mirror does make a major difference to the detailed intensities of the inner PSF structure and the relative intensities of the main diffraction spikes (see Figure 1). The PSF has three distinct ‘zones’: the inner very bright few pixels, a ring of 12 complex knots and ‘streamers’ out to radii of about 0.3 arcsec (at our filter wavelengths), and four diffraction spikes that are seen to large radii. In our PSF-fitting, we found the inner few pixels cannot be fit well, partly due to saturation effects in the data, and anyway contain no resolved information. Thus, the criteria for choosing the PSF model are the relative brightnesses of the ring of knots and the long spikes. A best model was selected from a grid of secondary mirror offsets for each QSO and filter. The model grids were done with a coarse grid and a finer grid near the best-looking value. The PSF model selection was done by inspection and then by minimising the residual structure in the PSF-subtracted QSO images. It was found that the same model offsets (close to 1mm in both x and z) were selected for all QSOs and both filters, independently by the first two authors. These were significantly better than Tiny Tim or a simple mean PSF from our grid of observations, in matching the detailed structure seen in the QSO images.

After selecting the best-looking PSF model, it was block-averaged by a factor 8, using a grid of 8 x 8 single (fine) pixel offsets. This enabled us to match the pixel sampling of the QSO, which was judged by the sampling of the four triple-stripe diffraction spikes. These spikes are about one PC pixel wide. This was the PSF used with matched sampling to the data, for subtraction from the QSO images. We found that the subtraction results do not change rapidly within 1mm offset steps, so that selection of the ‘best’ model was not critical within a range of about 0.3mm in the offsets.

The PC-pixel sampled PSF was then scaled and subtracted from the QSO image. In all cases a grid of scale factors (and pre-block-averaging PSF shifts) was used to decide which was the best PSF subtraction. In choosing the best subtraction, the subtracted image was modelled for its fit to exponential and de Vaucouleurs law azimuthally averaged profiles. The subtracted images were characterised by using the ‘ellipse’ task in IRAF, centred on the nucleus position. The fits were judged by minimising profile differences from the two types of model - i.e. linearity in $\log(\text{signal})$ against radius or $\text{radius}^{1/4}$. We gave zero weight to the innermost 4 pixel radius (about 0.65 in $\text{R}^{1/4}$ in Figure 3), which lie inside the resolution of the images and where there are saturated pixels; and a weight inversely proportional to the error bars calculated from the image by the ellipse task. In the diagrams and plots, we have interpolated across the low pixels in the inner 4 pixel radius, resulting in an apparent excess of unresolved flux in the central pixels. We stress that there is no information in

these pixels and they are not taken into account in the measured quantities. Best fit models are extrapolated into the central few pixels in deriving the quoted host galaxy fluxes.

We also inspected the 2-dimensional subtracted images for residual PSF structure. This was already minimised in morphology by the PSF model selection, but visual inspection is sensitive to under- or over-subtraction that might not show up in azimuthally averaged profiles. The final adopted subtractions were a mean of the profile fits and image structure inspection values for scaling, but these were always the same within a few percent in the final resolved flux estimates.

Finally, the sensitivity to the PSF models, positions, and scaling were tested by finding best fits over a range of each of these parameters. The PSF-subtracted fluxes were robust to within 10% - i.e. for the range of fits that are acceptable by the above criteria. The host galaxy structures outside radii of 0.5 arcsec are not sensitive to any of the fit parameters explored, while structures and total signal level inside this depended on the relative nuclear to host flux ratio, as discussed individually below.

Figure 2 shows an example of PSF-subtraction from a PSF-star image. The diagram illustrates that the central region is not properly modelled (by choice, as noted above), and that no detectable flux is seen in the subtracted image beyond radius 0.35''. This PSF fit is not as good as those for the QSOs, as the short PSF-star exposures suffer from telescope breathing and worse read noise than the longer QSO integrations, and are from different places on the detector, so we did not attempt very detailed modelling for the individual PSF observations. Nevertheless, we note that all the QSOs showed more extended and significant resolved structure than the star image in Figure 2.

For each PSF-subtracted QSO image, we calculated (and tabulate) the total flux from the best-fit model, which interpolates across the central pixels as shown in the diagrams. The values agree well with the summed image signal within the radius limits of good fit. *In all cases we found much better fits for the inner host galaxies with a de Vaucouleurs model, but in most cases this did not fit well beyond a radius of about 0.8 to 0.9 arcsec.* Beyond this, we applied an exponential model fit: a different de Vaucouleurs model fit as well, but gave about the same total flux, and we consider the outer galaxy more likely to be an exponential anyway. We also note that the images show that the host galaxies are not at all symmetric ellipses, so that *we are using the de Vaucouleurs models as flux estimators rather than morphology discriminators.*

We describe the results for each QSO in the sections below. Table 2 summarizes the adopted best-fit subtractions and the measured or model quantities from them. The diagrams show subtracted images and luminosity profiles for all the objects. The plots have

limiting surface brightness of about 27 mag/arcsec². With smoothing it is possible to go about a magnitude fainter at radii about 3 arcsec, but the signal is poor and very sensitive to the sky level uncertainty. Note that we have used cosmological parameters $H_0=100$ and $q_0=0.5$ in quoting absolute magnitudes, with no K-correction applied.

We recorded the fluxes and positions of all galaxies measurable in both filters in the PC field surrounding the QSO. As all exposures and QSO redshifts are similar, this is a reasonably good comparison of the galaxy environments of the sample QSOs, in terms of richness and galaxy colours, down to F602W magnitude ~ 26 . However, this part of the work is not a rigorous or flux-limited investigation of the QSO companions, as we were unable to measure fainter or LSB objects that were visible in some fields.

4. Notes on individual QSOs

4.1. 0033+098

The QSO is radio-loud (460mJy at 5 GHz: Pauliny-Toth et al 1972), but with no known radio structure. The QSO was fainter than the catalogued $V=17.5$ (Hewitt and Burbidge 1993) suggests, with $R=18.9$ and $I=18.6$. We have measured several nearby faint galaxies, and most have similar colours (see Table 2).

Figures 3 and 4 show the images and luminosity profiles for the QSO. The best-fit de Vaucouleurs model is shown, as discussed in the previous section. In fact, the QSO host galaxy appears to be asymmetrical and to contain knots, so the assumption of a smooth de Vaucouleurs profile is not necessarily the best way to measure the host galaxy. The ‘ellipse’ IRAF task used can be used to fit an ellipse to successive mean radii with a free centroid, so that the effect of departures from azimuthal symmetry are minimised, while allowing us to quantify deviations from central symmetry by the migration of successive ellipse centroids.

In both F606W and F702W images, the de Vaucouleurs fit was good out to a radius of about 1''. Beyond that, there is excess light that may be approximated better by an exponential disk (or different de Vaucouleurs model), out to about 2'' radius. Beyond that, the signal is too weak to measure. This illustrates a generic point well: HST has good resolution and signal in the radius range 0.2'' to 1.0''. Ground-based observations with larger telescopes reveal flux extending to several arcsec in many such objects. Thus, HST is measuring the central spheroidal-like population of the host galaxy, but may fail to detect a more extended disk, arms, or halo. Our deep HST images just cover the transition between these regions.

The host galaxy does have asymmetrical structure that is seen (Figure 1) as an extension to the top of the image, plus a separate knot to the left side. The fitted ellipses have centroids that move systematically by several pixels from the nucleus to the outer contours, reflecting this. Note too that the visible structures lie within the radius fit by the de Vaucouleurs model, so that the ‘bulge’ model fit does not imply the presence of a smooth bulge in the conventional sense. These structures are faint, but the overall resolved flux from the host galaxy indicates a high luminosity, which is several magnitudes brighter than any of the nearby galaxies, and corresponds to absolute magnitude $M_R \sim -25$. This is similar to measurements of other radio-loud QSO hosts at redshift near 2.

Table 2 summarizes the measurements of this and the other QSO fields. Other galaxies seen in the PC frame are faint and compact, and are generally blue, with two exceptions at $R-I = 1.6$. In all the QSO fields we have not counted galaxies redder than $R-I=1.0$ in Table 2. The other fields have only one such red galaxy each, so they form a minor part of the companion totals. The flux from the extended structure to the N of the QSO, measured on its own, is also blue, with $R-I$ close to 0.0. The ‘companions’ range in luminosity from our Galaxy to the LMC if at the QSO redshift. They are all blue enough to be star-forming at the QSO redshift or higher. Sizes range from small to moderate (0.3 to 1.5 arcsec) to the brightness level detected. The space density at the QSO redshift is high.

4.2. 0225–014

This is a radio-loud QSO (4C 01.11: 300mJy at 2.7GHz, 150mJy at 5GHz: see e.g. Barthel et al 1990). It has C IV absorption at $z=2.0$. It is a triple radio source (17” long) with a 35° bend, and an overall spectral index fairly steep at 1.1. Table 2 shows the measured quantities for the QSO and associated objects. The QSO host galaxy is resolved and has quite asymmetric structure. The PSF removal works well outside the central 6-7 pixel diameter, and is shown in Figures 3 and 4.

The azimuthally averaged profile from fitting ellipses to the PSF-subtracted QSO fits a spheroidal model fairly well, but there are significant bumps and dips in the profile. The outer parts (beyond radius 0.8”) in the F606W image can be fit to an exponential profile, and the spheroid model does not fit in the F606W filter. Thus, there may be a faint halo or ‘disk’ that we are just detecting. In the F702W image, the arm is less conspicuous and the disk component is not indicated: a spheroidal model fits to the radius limit of the image. We stress that these model fits are useful in estimating the resolved total luminosity but do not indicate the presence of normal bulge or disk morphology. The resolved flux is one-sided and contains a curved bright arm that extends almost 1” from the nucleus. The centroids of

the ellipses move some 0.2" from the nucleus to mean radii of 0.7" as they include this arm.

The radio structure has only 1.4" resolution but shows an extended core (jet?) whose direction is along the brightest HST diffraction spike residual. Thus, our host galaxy detection is poorest along this line. The curved arm of the host galaxy appears to originate at this angle. The radio lobe peaks lie within the surrounding group. The NW lobe is along the jet direction and is further from the nucleus by about a factor 2. It does not correspond with any detected optical source. The SE lobe is extended perpendicular to the radius to the QSO and lies near the edge of the group of galaxies, close to (but not on) a diffuse large faint galaxy.

The QSO lies in a field of faint companions. 26 are seen in the PC chip (although only 16 were measured reliably in both filters), which is about double that seen in others in the sample. The companions are grouped within the PC field, with the QSO off-centre. Only one or two have colours that suggest they are foreground - the rest are very blue and thus may be star-forming at high redshift. The galaxies range from very compact to small and nucleated, many with very asymmetrical structure. Unusually, there are also several (7) which are large, LSB, and not nucleated at all. The largest is blue and quite luminous.

The QSO appears to be part of a group of young galaxies or protogalaxies and to be in a host galaxy that is large and irregular, with low surface brightness features. In view of the absorber seen at the slightly lower redshift of 2.0, some (or all?) of the resolved structure and of the companion galaxies may lie in this group at a few thousand km/s lower redshift than the QSO.

4.3. 0820+296

This is a radio-loud QSO that has been imaged with the CFHT in earlier work (see Hutchings 1995 a,b and references therein). The ground-based visible imaging at 0.6" FWHM resolution indicated that the QSO is extended azimuthally at radii 1.5" to 4". The QSO was also found to have a high count of nearby galaxies at projected distances 20-30", with magnitudes complete to about R=24. Many of them are blue, and were discussed in terms of star-forming companions at redshifts similar to the QSO. The QSO spectrum contains absorptions at $z \sim 2.05$, so the galaxies may be part of that absorbing group.

The resolved light in the F606W filter has a ring-like structure, somewhat offset and with brightness that changes around the ring. The F702W image shows this less clearly but has more resolved light overall. Figure 2 shows the luminosity plots and the adopted spheroidal models that fit them best (but with significant irregularity in the profile). The

F702W image also has a halo or outer disk beyond a radius of 0.9''. This is seen less significantly and with less light in the F606W image. It is possible that this galaxy has a ring of new star-formation plus an older population, indicating an event that triggered the QSO episode.

The WFPC2 images show fainter galaxies than the ground-based (about 1 magnitude, where they are compact). This changes the selection criteria for galaxy counts from those in the CFHT study. There are 12 measured in both colours on the PC chip, plus one star which is the brightest and reddest object. One galaxy is red (and bright) and is likely to be foreground. The rest are all blue and thus possibly star-forming at high redshift, as noted in the CFHT study.

4.4. 1338+277

The QSO is radio-quiet, discovered in the Crampton et al (1995) survey. They note it is extended. The QSO was imaged with the CFHT (Hutchings 1995 a,b) with 0.8'' FWHM image quality. The azimuthally averaged profile is resolved at radii 1-3'', and a knot 1.2'' to the North is noted. There appears to be some excess of galaxies to $R=24$ around it to radii approx 30''.

The new data show the QSO is faint (about 21.5 magnitude) and the HST images have little visible PSF structure. The QSO is non-circular down to very small radii (0.2''), and has faint flux with elliptical contours out to some 0.6''. The images also clearly show a jet-like extension at some 60° to the inner structure, extending some 1.4'' and ending at a brighter knot (see Figure 3). The knot is more compact in F606W and there is an apparent gap between the 'jet' and knot.

The elliptical inner host extension is blue and the inside part of the jet is red. The QSO has R magnitude 1.6 fainter than the catalogued V value of 20. The jet is 26.7m and the blue region comparable. The 'bulge' component is as shown by the plotted models and the 'disk' is an additional exponential beyond radius 0.7''. These fits produce reliable total flux values, but are clearly not good fits to the morphology.

The PC chip contains 12 companion objects, measured in both filters. The QSO is the brightest object in the PC chip. The companions are small and faint, with 2 exceptions, but all could be galaxies at the QSO redshift. All but one (which is also one of the two larger ones) are blue objects, so consistent with their being true companions. The area of sky covered by this group is within the PC field - about 180 Kpc on a side - so that this is a high concentration. The galaxies have luminosities like the LMC or M33 if at the QSO

redshift and with low k-correction.

4.5. 2244–010

This is an LBQS object (Foltz et al 1989), so has a luminous nucleus, and is the brightest in our sample by over a magnitude. It has associated absorption in the C IV and L alpha profiles (not BAL, but narrower). Little else seems to be known, and no radio detection is reported.

The HST images show very little structure and the bright nucleus makes imperfections in the PSF modelling and subtraction more significant. Our best PSF subtractions suggest a small compact knot about 2.5arcsec to the West, but otherwise no obvious structure beyond diffuse extended light through the PSF features. Figure 4 shows that there is no good fit to a spheroidal model, especially at the shorter wavelengths. An exponential works moderately well beyond radii of 0.8 arcsec. The host galaxy light is redder than the nucleus, and similar to other faint galaxies in the field.

There are several faint and compact companions, all blue enough to be at the QSO redshift. One galaxy is red (and larger) and is presumably foreground. One other largish (chain?) galaxy is blue and quite luminous if at the QSO redshift. The spatial distribution is even over the PC chip, and thus not obviously clustered around the QSO. The companions range from very compact to diffuse with no nucleus (but still small).

5. Discussion

Our new PSF models have been instrumental in achieving improved resolution and modelling of the inner parts of high redshift QSO hosts. However, there are still PSF artifacts that are not properly removed, most obviously in the brightest of our targets. It is not straightforward to quantify our errors. We have covered a wide range of PSF shifts and scale factors, as well as PSF models in this work, and consider that the resolved flux values quoted are robust to a level of 10% in all cases.

Table 2 compares the principal results for the sample. Since the QSOs are all at similar redshift and have similar exposures, the spatial scales and apparent colours may be compared directly, as well as properties of companions. In the Table 2 summary, we have removed all companion galaxies that are redder than $R-I=1$ mag, supposing that they may be foreground objects. There are few of these and the average numbers are little affected by their removal.

In all cases, the bulk of the resolved light is best fit by a spheroidal type of profile, but in all cases this requires an extra component which we have modelled with an exponential, beyond radii of about 0.8" (corresponding to about 4Kpc in the adopted cosmology). This statement is robust against uncertainties in the sky level, which affects only the outermost 2 or 3 points in our plots. The exponential light is faint and only its innermost parts are detected in our data. In ground-based observations with larger telescopes (e.g. Hutchings 1995a), the faint outer light is often resolved out to several arcsec, further reinforcing the model of a two-part light distribution for these galaxies, which we can ‘fit’ with spheroidal and disk models. However, the morphology is in all cases irregular within the radius of bulge model fit, and indeed some of the luminosity profiles themselves are irregular, so we do not simply interpret the azimuthally averaged profiles in terms of bulge and disk components seen in regular galaxies in the local universe, and do not conclude that the host galaxies are all ‘elliptical’. We also note that less deep HST imaging would fail to detect any of the outer ‘disk’ light. As noted by Hutchings (2001a,b) we should thus be cautious of claims that HST data reveal that high redshift QSO hosts are all ‘elliptical’.

The resolved flux, however, is quite well measured by these models, and is 2-3 magnitudes more luminous than L^* in the local universe. The colours are blue, and with rest wavelengths in the NUV, indicate that the light is dominated by massive young stars. Note that the k-corrections for a young population at this redshift are negative, but the amount depends on the age (and reddening) of the young stellar population present. Thus, comparison with present epoch standard galaxy luminosities is not very meaningful. If free of dust, and evolving passively without further merging events, the QSO host galaxies would become present day galaxies of about L^* luminosity.

There is no difference between radio-loud and radio-quiet QSO hosts in our small sample, but the two radio-quiet QSOs are the brightest and faintest of the group, and their discovery techniques (LBQS and faint optical search) certainly bias the comparison. The QSO R and I magnitudes of four of the group are sufficiently fainter than their catalogued V magnitudes, that they must have varied. Overall, the resolved light lies close to 10% of the QSO for all objects, averaging the V, R, and I values.

The relationship between bulge luminosity and central black-hole mass in galaxies in the local universe has been used to claim that high mass black holes are required for radio-loud QSOs (e.g. McLure and Dunlop 2001a,b, Dunlop et al 2001). Since the epoch of initial formation of the black hole and the ‘bulge’ population are both unknown, as well as their subsequent change with time, this too should be treated with caution. In addition, there is evidence that there is a continuum of radio power in lower redshift QSOs (Lacy et al 2001), as well as systematic changes in radio morphology with redshift (Neff and

Hutchings 1990), so a simple dichotomy may not apply at high redshift either. Perhaps a more direct indication of black hole mass is the broad-line width, but here too we need to understand the kinematics of BLR, as well as its cosmic evolution.

The irregular morphology of 4 of the five objects suggests that the host galaxies may be in the process of hierarchical formation, or other tidal events, as well as associated with very active star-formation. This is similar to the conclusions of other investigations of $z \sim 2$ QSOs. The HST data have revealed structure of subarcsecond size, within 1-2 arcsec of the QSO nucleus that support and add to this scenario. These results reinforce the caveats noted above.

To the extent that the central black hole mass is related to the initial stellar population in a galaxy (which in the present day universe is the spheroidal, or non-disk, part of all galaxies), we may expect the entire QSO host galaxy luminosity to be related to the central black hole mass, at these redshifts where galaxies are very young, regardless of whether the morphology is strictly spheroidal. However, the proportionality factor of stellar luminosity to central mass may well change as the galaxy evolves (and undergoes merging) over its lifetime. We expect the spheroidal population luminosity to decline with time, with possible boosts by major mergers, while the black hole mass can only increase - perhaps by a large factor.

One way to check this independently is the widths of the nuclear broad emission lines, as discussed by McLure and Dunlop (2001a), among others. In our sample, there are 3 with published spectra, and these are not of very good quality for line width measures. The spectrum of 2244-010 (Foltz et al 1989) shows it to have significant shortward absorptions to the broad lines, but we estimate the width of the unabsorbed emission to have FWHM of 7000 km.s^{-1} . We measure profiles in 0033+098 (Steidel and Sargent 1991) and 0820+296 (Maoz et al 1993) to have FWHM 5400 and 3900 km.s^{-1} respectively. In this small sample we see no correlation with the host galaxy luminosity, or radio luminosity.

The distribution of faint blue galaxies near the QSOs is similar for all, with the exception of 0225-014, which has a much higher fraction of companions within 10 arcsec (Table 2 gives the galaxies within the entire ~ 37 arcsec field of the PC). As a rigorous investigation of the distribution and detection criteria for companions seems unprofitable, we have not pursued these statistics further.

Further progress awaits a large and uniform investigation of high redshift QSO hosts, with high sensitivity as well as spatial resolution. New instrumentation on HST as well as 8m class ground-based telescopes, offer excellent opportunities for such studies.

References

Crampton D., Schade D., Cowley A.P., 1995, AJ, 90, 987

Dumont P.J., Redding D.C., Love, S., Boden A., Hanisch R.J., Mo J., 2001 (in preparation)

Dunlop J.S., McLure R.J., Kukula M.J., Baum S., O'Dea C.P., Hughes D.H., 2001 MNRAS (in press: astro-ph 0108397)

Foltz C.B., Chaffee F.H., Hewett P.C., Weymann R.J., Anderson S.F., MacAlpine G.M., 1989, AJ, 98, 1959

Heckman T.M., Lehnert M.D., van Breugel W., Miley G.K., 1992, ApJ, 370, 78

Hewitt A., and Burbidge G., 1993, ApJS, 87, 451

Hutchings J.B., 1995a, AJ, 109, 928

Hutchings J.B., 1995b AJ, 110, 994

Hutchings J.B., 2001a, astro-ph 0107157

Hutchings J.B., 2001b, IAU colloquium 184 (in press)

Krist, J. 1995, ASP Conf Ser 77 (ADASS IV), R. A. Shaw, H. E. Payne, & J. J. E. Hayes, eds., p. 349

Kukula M.J. et al 2001 MNRAS (in press: astro-ph 0010007)

Lacy M., Laurent-Muehmeisen S.A., Ridgway S.E., Becker R.H., White R.L., 2001

Lehnert M.D., Heckman T.M., Chambers K.C., Miley G.K., 1992, ApJ, 393, 68

Maoz D., Bahcall J.N., Schneider D.P. et al 1993, ApJ, 409, 28

McLure R.J., Dunlop J.S., Kukula M.J., Baum S.A., O'Dea C.P., Hughes D.H., 1999, MNRAS, 308, 377

McLure R.J., and Dunlop J.S., 2001a, MNRAS, 327, 199

McLure R.J., and Dunlop J.S., 2001b, astro-ph 0108417

Neff S.G., and Hutchings J.B., 1990, AJ, 100, 1441

Pauliny-Toth I.I.K., Kellerman K.I., Davis M.M., Fomalont E.B., and Shaffer D.B., 1972, AJ, 77, 265

Ridgway S.E., Heckman T.M., Calzetti D., Lehnert M., 2001, ApJ, 550, 122

Steidel C.C. and Sargent W.L.W., 1991, AJ, 102, 1610

Captions to figures

1. PSF models with different offsets of HST secondary mirror. The offset difference is 2 mm. Note the significant changes in the brightness of the inner ring of spots and the components on the main diffraction spikes. A grid of these models was used to match the structure seen in the QSO images.
2. PSF-star images to illustrate subtraction. The PSF model and star image are shown in the top row, matched in pixel sampling, and the subtracted image is below. The images are 3.2 arcsec on a side. The text notes that this PSF subtraction is not as good as for the QSO images.
3. Images of the program QSOs, 2.8 arcsec on a side. These are after optimal PSF subtraction, as described in the text, and are combined from the two filter images. The images have been smoothed with a 0.037 arcsec gaussian to reduce pixel noise. The saturated inner cores in most of them are dominated by PSF artifacts but the core of the faint QSO 1338+277 is resolved. Note the asymmetric structures, the knot to the left of 0033+098 and the ‘jet’ of 1338+277. Faint traces of the diagonal diffraction spikes are seen in some images. North is 126° clockwise of up for 0033+098; 17° anticlockwise for 0225-014; 85° clockwise for 0820+296; 100° clockwise for 1338+277; 30° clockwise for 2244-010.
4. Luminosity profiles of sample QSOs. Top left shows full QSO image showing it is resolved compared with the PSF. The other profiles are after PSF subtraction. Lowest levels plotted are close to 27 mag per square arcsec. The excess light within $r^{1/4} \sim 0.65$ is not significant and ignored in estimating the host galaxy fluxes. The dotted lines are the spheroidal models used to calculate the ‘bulge’ fluxes. Excess light above these lines at larger radii is fitted with an exponential to calculate the detected ‘disk’ components.

Table 1. Observations

Name	Mag ¹	z	Date	F606W ²	F702W ²
0033+098 ³	17.5	1.91	Nov 22 1998	4650	5200
0225–014 ³	18.2	2.04	Nov 12 1998	5000	5400
0820+296 ³	18.5	2.37	Feb 20 1999	5300	5400
1338+277	20.0	2.28	Feb 14 1999	5300	5400
2244–010	18.0	2.03	May 15 1999	5000	5400
Feige 23	11.1	0	Oct 24 1998	~900	~900

¹Catalogue V magnitude

²Exposure time in seconds

³Radio-loud QSO

Table 2. Summary of results

	0033+098	0225-014	0820+296	1338+277	2244-010
F606W					
Total	18.9	18.7	19.1	21.5	17.6
Bulge	20.1	21.3	21.3	23.1	20.6
Disk	22.9	23.9	24.3	24.6	22.9
Bulge/Total	0.36	0.09	0.14	0.23	0.06
F702W					
Total	18.6	18.6	19.2	21.6	17.5
Bulge	20.2	21.3	21.1	23.5	20.0
Bulge/Total	0.24	0.08	0.17	0.17	0.10
QSO R-I	0.3	0.1	-0.1	-0.1	0.1
Bulge R-I	0.1	0.0	0.2	-0.4	0.6
Bulge M_R^a	-24.7	-23.8	-24.1	-22.3	-24.5
Disk M_R	-21.9	-21.2	-21.1	-20.8	-22.2
Comp# ^b	3/10	6/15	3/11	4/11	2/12
Comp dist (") ^c	15±4	13±5	14±5	12±4	15±5
Comp mag ^d	24.6±1.0	25.0±0.8	24.0±1.2	24.7±0.4	25.1±1.0
Comp R-I ^e	0.24±0.58	-0.1±0.43	0.2±0.3	0.0±0.34	0.25±0.33
Comp mean M_R	-20.2	-20.1	-21.4	-20.7	-20.0

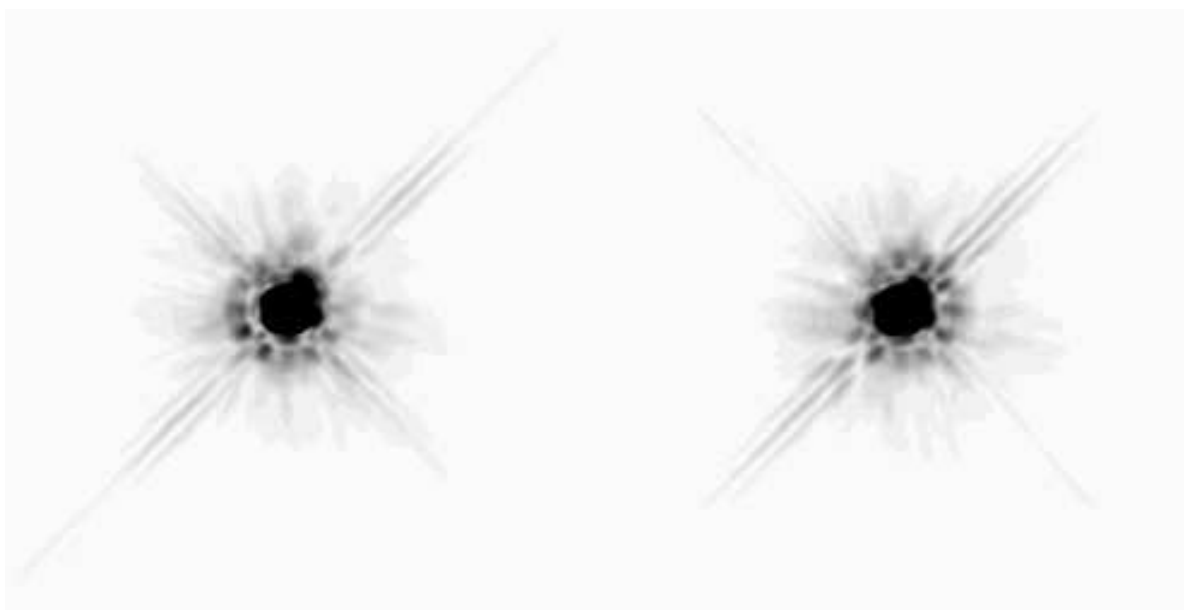
^aM values with no k-correction

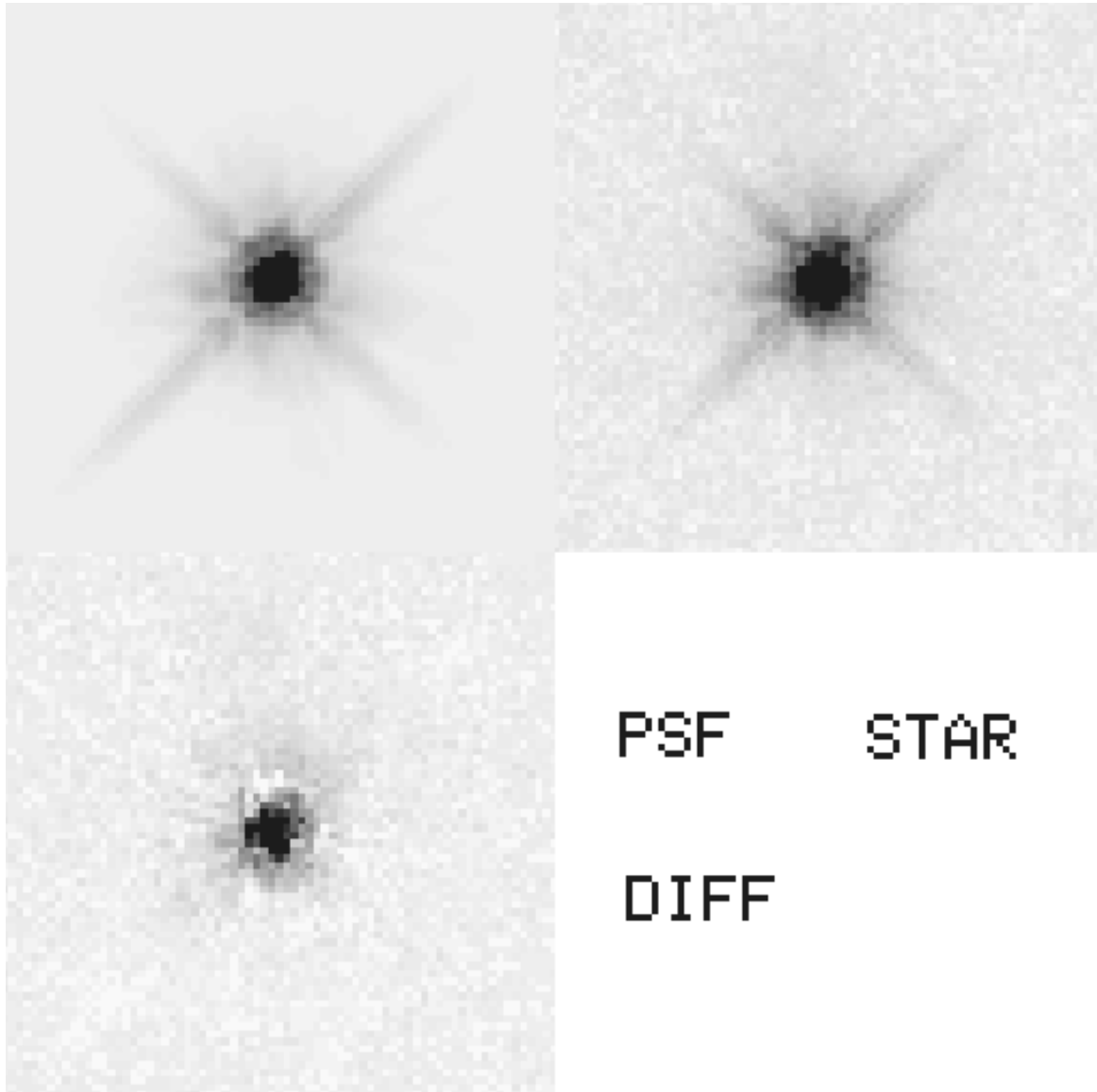
^bGalaxies in both filters, within 10" and over whole PC field

^cAverage offset from QSO in arcsec

^dAverage R mag of galaxies

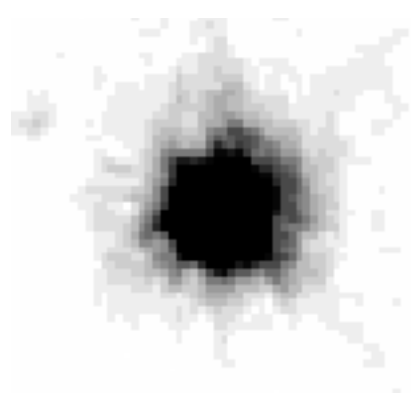
^eAverage R-I of galaxies <1.0 - i.e. w/o foreground



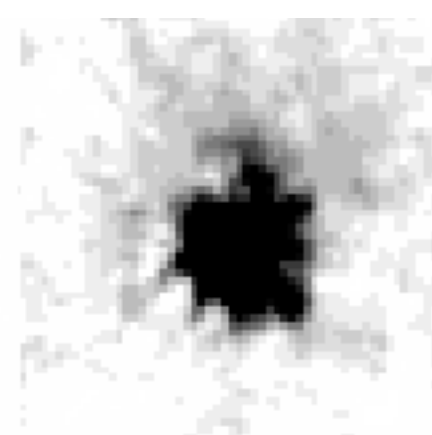


PSF STAR

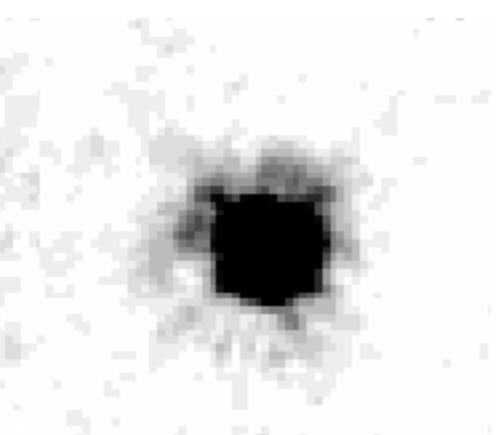
DIFF



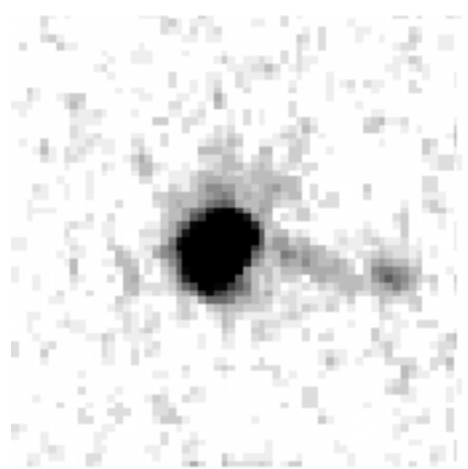
0033



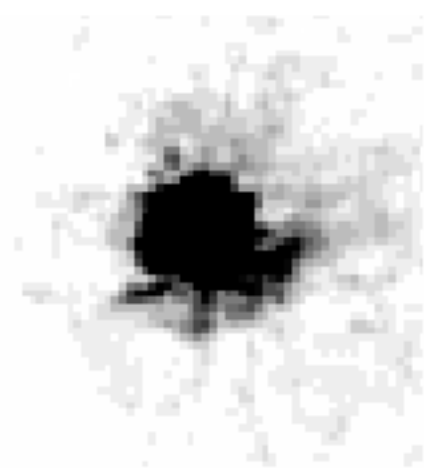
0225



0820



1338



2244

